Colloids and Surfaces B: Biointerfaces 111 (2013) 107–116

Contents lists available at SciVerse ScienceDirect

Colloids and Surfaces B: Biointerfaces

journal homepage: www.elsevier.com/locate/colsurfb

Peptide decorated nano-hydroxyapatite with enhanced bioactivity and osteogenic differentiation *via* polydopamine coating

Yuhua Sun[a,1], Yi Deng[a,b,1], Ziyou Ye[b,d], Shanshan Liang[e], Zhihui Tang[c,*], Shicheng Wei[a,b,c,**]

[a] *Department of Oral and Maxillofacial Surgery, Laboratory of Interdisciplinary Studies, School and Hospital of Stomatology, Peking University, Beijing 100081, China*
[b] *Center for Biomedical Materials and Tissue Engineering, Academy for Advanced Interdisciplinary Studies, Peking University, Beijing 100871, China*
[c] *2nd Dental Center, School and Hospital of Stomatology, Peking University, Beijing 100081, China*
[d] *School of Biology and Basic Medical Sciences, Medical College, Soochow University, Jiangsu 215123, China*
[e] *Department of Oral and Maxillofacial Surgery, School of Stomatology, Hainan Medical College, Hainan 571199, China*

ARTICLE INFO

Article history:
Received 17 April 2013
Received in revised form 11 May 2013
Accepted 25 May 2013
Available online xxx

Keywords:
Nano-hydroxyapatite
Peptide
Polydopamine
Bioactivity
Osteogenic differentiation

ABSTRACT

To be better used as implant materials in bone graft substitutes, bioactivity and osteogenesis of nano-hydroxyapatite (nano-HA) need to be further enhanced. Inspired by adhesive proteins in mussels, here we developed a novel bone forming peptide decorated nano-HA material. In this study, nano-HA was coated by one-step pH-induced polymerization of dopamine, and then the peptide was grafted onto polydopamine (pDA) coated nano-HA (HA-pDA) through catechol chemistry. Our results demonstrated that the peptide-conjugated nano-HA crystals could induce the adhesion and proliferation of MG-63 cells. Moreover, the highly alkaline phosphatase activity of the functionalized nano-HA indicated that the grafted peptide could maintain its biological activity after immobilization onto the surface of HA-pDA, especially at the concentration of 100 μg/mL. These modified nano-HA crystals with better bioactivity and osteogenic differentiation hold great potential to be applied as bioactive materials in bone repairing, bone regeneration and bio-implant coating applications.

1. Introduction

It is well known that bone is made up of collagen and nano-hydroxyapatite (nano-HA) in the form of needle-like or rod-like shapes [1]. Due to its good osteointegration, bone-binding property and biostability [2,3], HA biomaterial has drawn great interest in clinic, for example, as artificial bone and coatings on titanium prostheses surface. However, HA particles or wear debris from HA coating can cause inflammatory reactions, especially for the nano-size particles [4,5]. Nanosize HA was also reported to inhibit the growth of osteoblasts in a concentration-dependent manner. Xu et al. reported that the apoptotic and inhibition ratios of osteoblasts were rising with increasing of nano-HA concentration [6], and the similar results were found by Motskin and Fu et al. [7,8]. If osteoblasts die on the surface of implants because of the presence of nano-HA debris, the new bone will hardly be generated. Therefore, it is still critical to decrease and even eliminate the inhibition and apoptosis caused by nano-HA.

Many efforts have been devoted to HA modification to promote osteoblast adhesion, reduce infection rates and accelerate bone forming [9,10]. Such goals could be partially reached by activating the surface *via* plasma treatment [11]. Another method is to modify the surface with bioactive macromolecules. Extracellular matrix (ECM) proteins, including collagen [12], fibronectin [13], peptides [14] and bone morphogenetic proteins (BMPs) [15], have been actively investigated to improve the bioactivity of implant materials. Diverse approaches including physical adsorption and chemical covalent conjugation have been applied to immobilize ECM proteins or peptides onto implant material's surface. Physical adsorption is a simple process, however, simply adsorbed molecules are often released with a burst in the initial stage. Chemical conjugation is more effective for prolonged periods of

* Corresponding author at: 2nd Dental Center, School and Hospital of Stomatology, Peking University, Beijing 10081, China. Tel.: +86 1082196271; fax: +86 1082196271.
** Corresponding author at: School and Hospital of Stomatology, Peking University, No. 22 Zhong-Guan-Cun South Road, Hai-Dian District, Beijing 100081, China. Tel.: +86 10 82195780; fax: +86 10 82195780.
E-mail addresses: tang_zhihui@live.cn (Z. Tang), sc-wei@pku.edu.cn, weishicheng99@163.com (S. Wei).
[1] Both these authors contributed equally to this work.

0927-7765/$ – see front matter © 2013 Elsevier B.V. All rights reserved.
http://dx.doi.org/10.1016/j.colsurfb.2013.05.037

time, allowing successive regulation of cell behaviors [16]. However, typical chemical conjugation methods require multistep, complicated procedures such as surface activation or functionalization steps requiring plasma or chemical treatments [17,18]. Furthermore, denaturation of bioactive molecules by toxic chemicals and multiple reaction steps may be an additional issue to be addressed, which restricts its applications in clinic [19].

BMPs are the most potent growth factors for enhancing bone formation [20,21] and are also reported to be involved in various biological processes, including cell differentiation, proliferation, and migration [22,23]. Especially, BMP-7 has been proven to play a crucial role in modulating osteogenic differentiation and proliferation at the biomaterial–tissue interface and in promoting osseointegration [24,25]. Nevertheless, the complex multilevel structure of BMPs renders them prone to degradation, and they tend to lose their bioactivity quickly in physiological conditions [26]. A short functional peptide derived from BMPs has the potential to increase the efficacy of BMP delivery. Recently, Kim demonstrated that a new bone forming peptide sequence (GQGFSYPYKAVFSTQ) from BMP-7 had more osteogenic activity than BMP-7 and induced osteogenesis [24].

Dopamine (DA), a mussel inspired molecule, could undergo self-polymerization and adhere onto almost any solid surface in alkaline solution without surface pretreatments [19,27,28]. More importantly, polydopamine (pDA) coating can function as anchors to graft the secondary functional biopolymers by thiols and amines *via* Michael addition or Schiff base reactions [27]. Recently, researchers have devoted to develop a facile coating method based on dopamine to immobilize nano-HA coating on implants materials to improve osteointegration, such as titanium and polyglycolic acid, and they have achieved the promising osteogenic results for bone tissue engineering [29,30]. However, the puzzling problem, that nano-HA particles or wear debris from HA coating cause inflammatory reactions, has not yet been resolved. To this end, decreasing and eliminating the inhibition and apoptosis of nano-HA on the osteoblasts are desired. Herein, in the study, we present a novel peptide decorated nano-HA crystals with enhanced bioactivity and osteogenic differentiation ability for the first time. In the method, nano-HA was coated by a pDA layer, and then the new bone forming peptide was grafted onto pDA functionalized nano-HA through catechol chemistry. Fourier transform infrared spectrometry (FT-IR) and X-ray photoelectron spectroscopy (XPS) showed that the peptide was successfully grafted onto the surface of nano-HA. The effects of the peptide functionalized HA on cell viability and apoptosis were investigated. Moreover, the osteogenic differentiation activity of the decorated nano-HA was also studied. The presented facile and green method confers the poorly bioactive nano-HA crystals with both enhanced bioactivity and osteogenic differentiation, and the new modified nano-HA holds great potential for bone graft substitutes and bio-implant coating applications.

2. Materials and methods

2.1. Materials

3,4-Dihydroxyphenylamine was purchased from Sigma (St. Louis, USA). To facilitate chemical conjugation onto material's surface, peptide was modified at its N-terminal with a lysine-containing spacer. The peptide [KGGQGFSYPYKAVFSTQ sequence], provided by Chinapeptides Co., Ltd. (Shanghai, China), was synthesized by a batchwise fmoc-poly-amide method to more than 98% purity. Tris–HCl was purchased from Aladdin reagent Co., Ltd. (Shanghai, China). $Ca(NO_3)_2{\cdot}4H_2O$, $(NH_4)_2HPO_4$ and $NH_3{\cdot}H_2O$ were provided by Sinopharm Chemical Reagent Co., Ltd. (Beijing, China). All other chemicals were of analytical reagent grade and were used as received unless noted. All aqueous solutions were prepared with de-ionized water (D.I. water).

2.2. Synthesis of nano-HA

Firstly, $Ca(NO_3)_2$ and $(NH_4)_2HPO_4$ were dissolved in D.I. water separately according to a Ca/P molar ratio of 1.67/1. The pH of each solution was adjusted to 10 by adding ammonia. Then, $Ca(NO_3)_2$ solution was dropped into $(NH_4)_2HPO_4$ solution with continuous stirring. Crystal growth occurred when kept at 60 °C for 8 h, and the pH value of the supernatant was maintained in the range of 10–10.5 using ammonia. After reaction, HA slurry was kept at room temperature for 24 h, and the precipitate was obtained after washing with D.I. water and ethanol. Finally, HA precipitation was treated hydrothermally at 140 °C under 0.3 MPa for 20 h in an autoclave. After hydrothermal treatment, the nano-HA particles were rinsed with D.I. water and dried in an oven at 60 °C for 12 h.

2.3. Preparation of peptide functionalized nano-HA

pDA coated HA crystals (HA-pDA) were synthesized according to the following method: 500 mg nano-HA was immersed into 1L dopamine solution (2 mg/mL in 10 mM Tris–HCl, pH 8.5) and treated by sonication for 30 min. The mixture was stirred vigorously for 12 h at 60 °C, and then the reaction was stopped by centrifugation at 6000 × *g* for three times, followed by dialysis in D.I. water for 2 days to remove the unattached dopamine molecules.

The peptide functionalized nano-HA was prepared as following: 10 mg HA-pDA was added into 20 ml peptide solution (1× PBS) with different concentration (0.1, 0.5 and 1 mM) by a mild sonication for 10 min. Then the peptide grafting reaction was carried out at 25 °C for another 24 h with vigorous stirring. After that, the solution was centrifuged and thoroughly washed with D.I. water at 10,000 × *g* for three times, and dialyzed in D.I. water for two days to make sure that physically adsorbed peptide was removed completely. According to the different concentrations of peptide solution (0.1, 0.5 and 1 mM), the obtained decorated nano-HA was named as HA-0.1pep, HA-0.5pep and HA-1pep, respectively.

2.4. Morphology and structure characterization

Microstructural characterization was carried out using Tecnai F20 transmission electron microscope (TEM) with an accelerating voltage of 200 kV. Selected area electron diffraction (SAED) and Energy dispersive X-ray spectroscopy (EDX) were also recorded using the same equipment. The crystalline phase of the prepared powders before and after pDA coating were examined by X-ray diffraction (XRD, Shimadzu, Japan) using a Cu target as radiation source (λ = 1.540598 Å) at 40 kV. The diffraction angles (2θ) were set between 20° and 60°, incremented with a step size of 4 °min^{-1}. Thermo-gravimetric studies (TG, Q600, USA) were carried out to determine the actual yield of pDA on the surface of HA, and approximately 5 mg powders were heated from 25 °C to 900 °C with a heating rate of 10 °C/min under a nitrogen atmosphere. Fourier transform infrared spectrometry (FT-IR, Magna-IR 750, Nicolet, USA) was used to identify the functional groups of the samples, recorded from 400 cm^{-1} to 4000 cm^{-1}. Raman measurement was performed at 633 nm by using a Raman Imaging Microscope System (Renishaw 1000) in a backscattering geometry. X-ray photoelectron spectroscopy (XPS, AXIS Ultra, Kratos Analytical Ltd.) was employed to identify the chemical constituent and elemental state of prepared nano-HA. The binding energies were calibrated by the C1s peak at about 285 eV. Zeta potential measurements of the aqueous dispersions for the pristine nano-HA, HA-pDA

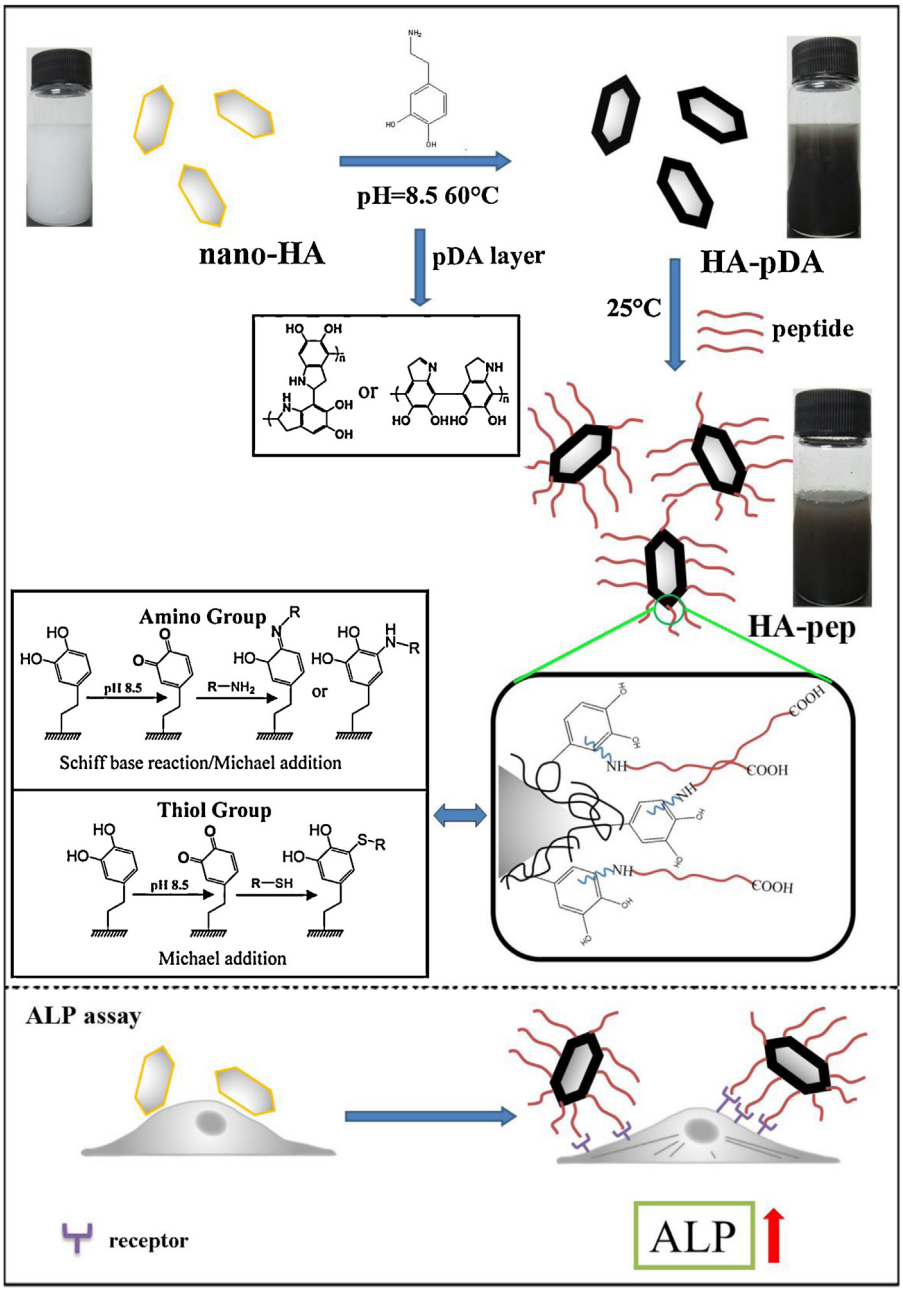

Scheme 1. Schematic illustration of preparation of the peptide decorated nano-HA by pDA coating and its ALP assay. The possible pDA chemical structure as well as the suggested reaction mechanism is also shown.

and the peptide grafted nano-HA were performed using Zetasizer ZS90 (Malvern Instruments Ltd., UK).

2.5. Cell culture

Human osteoblast-like MG-63 cells (American Type Culture Collection, VA, USA) were cultured in α-Modified Eagle's Medium (Gibco, Carlsbad, CA) containing 10% fetal calf serum (Gibco), 100 μg/mL streptomycin (Amresco, Cleveland, USA) and 100 μg/mL penicillin (Amresco) at 37 °C in a humidified atmosphere of 5% CO_2.

2.6. Cell viability assay

Viability of MG-63 cells was assessed using the cell counting kit-8 assay (CCK-8, Dojindo). After cell counting, MG-63 cells were seeded in 96-well plates (Costar, USA) at a density of 5×10^3 cells/well. After seeding 24 h, cells were rinsed with PBS buffer, and exposed to different functionalized nano-HA powders (100 μg/mL) and various concentrations (5, 10, 50, 100 and 500 μg/mL) of pristine nano-HA and HA-1pep. The control groups involved the use of DMEM medium as negative control and 10% DMSO DMEM medium as positive control. After incubating for 1, 3, 5 days, respectively, 10 μL of CCK-8 was added into each well for 4 h incubation. Then 80 μL of supernatant from each well was transferred to new 96-well cell culture plates. The absorbance value of supernatant optical density (OD value) was measured with a microplate reader (Model 680, Bio-Rad, CA).

2.7. FE-SEM observation of cells

MG-63 cells at 1×10^4 cells/mL were cultured on acid treated cover slips. The morphologies of MG-63 cells co-cultured with

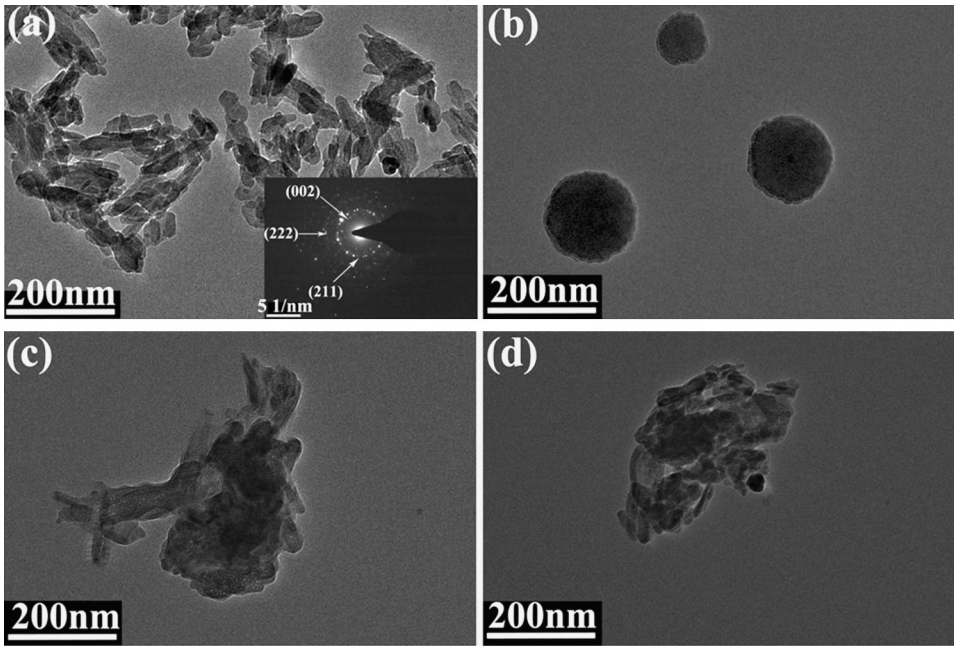

Fig. 1. Typical TEM images of pristine nano-HA (a), pDA (b), HA-pDA (c) and HA-1pep (d). The inset (a) shows the selected area electron diffraction (SAED) patterns of nano-HA.

different nano-HA were observed using a field emission scanning electron microscope (FE-SEM, 1910FE, Bedford, MA) after 3 days culture. All samples were fixed in 2.5% glutaraldehyde solution for 1 h and then dehydrated with graded ethanol solutions for scanning electron microscope testing. Dehydrated samples were dried by a vacuum dryer before sputter-coating with gold using a sputter coater.

2.8. Immunofluorescence

MG-63 cells at 1×10^4 cells/mL were cultured on acid treated cover slips. After 5 days, cells were washed with PBS and fixed with 4% (w/v) paraformaldehyde in PBS for 15 min at room temperature. The samples were then washed with PBS and permeabilized with 0.1% (v/v) Triton X-100 (Sigma) for 5 min, before being incubated with 1% bovine serum albumin/PBS at 37 °C for 30 min to block nonspecific binding. This was followed by adding 5 μg/mL FITC-phalloidin (Molecular Probes, Eugene, OR) to stain MG-63 cells for 30 min. After washed with PBS, samples were incubated for 5 min at room temperature with 10 μg/mL DAPI (Sigma–Aldrich). The stained signals in the cells were observed by a fluorescent microscopy (Carl Zeiss, Oberkochen, Germany). The number of adherent cells was determined by counting the number of nuclei at projected area (magnification 100×), and stained images were obtained from five different areas per sample ($n = 3$).

2.9. Apoptosis analysis

Cell apoptosis was analyzed by flow cytometry using an Annexin V-FITC apoptosis detection kit (Beyotime, Shanghai, China). MG-63 cells were cultured in 24-well plates at 5×10^4 cells/mL for 5 days. Then cells were digested with 0.05% pancreatic enzyme for 3 min. The digested cells were washed with the collected culture medium, and then suspended in PBS buffer. Cells were stained with the apoptosis detection kit according to the manufacturer's instructions. Briefly, the cells from each sample were suspended in 195 μL of Annexin V-FITC binding buffer, and 5 μL of Annexin V-FITC. The cells were incubated at room temperature for 10 min. Each sample was then centrifuged at $1200 \times g$ for 4 min, re-suspended in 190 μL of binding buffer and 10 μL of propidium iodide working solution was added. Then the samples were analyzed by a FACSCalibur (Becton Dickinson, NY, USA) flow cytometry with at least 10,000 events recorded for each condition.

2.10. Alkaline phosphate activity (ALP) assay

Alkaline phosphatase (ALP) activity of MG-63 cells was evaluated by an assay reagent kit (Nanjing Jiancheng Bioengineering Institute, China). At the end of the incubation, cells were exposed to the different functionalized nano-HA powders (100 μg/mL) and various concentrations (5, 10, 50, 100 and 500 μg/mL) of the pristine nano-HA and HA-1pep samples for 7 days. Briefly, the supernatant was removed and 100 μL of lysis solution (1% TritonX-100) was added into each well and incubated for 1 h. Afterwards, 30 μL of MG-63 cell lysates at each well was transferred to new 96-well cell culture plates, and cultivated with 50 μL of carbonated buffer solution (pH 10) and 50 μL of substrate solution (4-amino-antipyrine) at 37 °C for 15 min. Then 150 μL of potassium ferricyanide was added into the above solution, and the production of *p*-nitrophenol was determined by the absorbance at 405 nm. For normalization, the total protein concentration was measured by a Bicinchoninic Acid (BCA) protein assay kit (Beijing Biosea Biotechnology, China). Thus, alkaline phosphatase activity was normalized and expressed as the total protein content (U/gprot).

2.11. Statistical analysis

All data were expressed as mean standard deviations of a representative three similar experiments carried out in triplicate. Statistical analysis was performed with Origin software. Student's *t*-test was used to determine the significant differences among the groups, and *p*-values less than 0.05 were considered statistically significant.

3. Results and discussion

In this study, a facile biomimetic method was used to prepare a novel peptide decorated nano-HA with high bioactivity and osteogenic differentiation activity as schemed in Scheme 1. Briefly, HA nanocrystals were prepared *via* wet co-precipitation followed

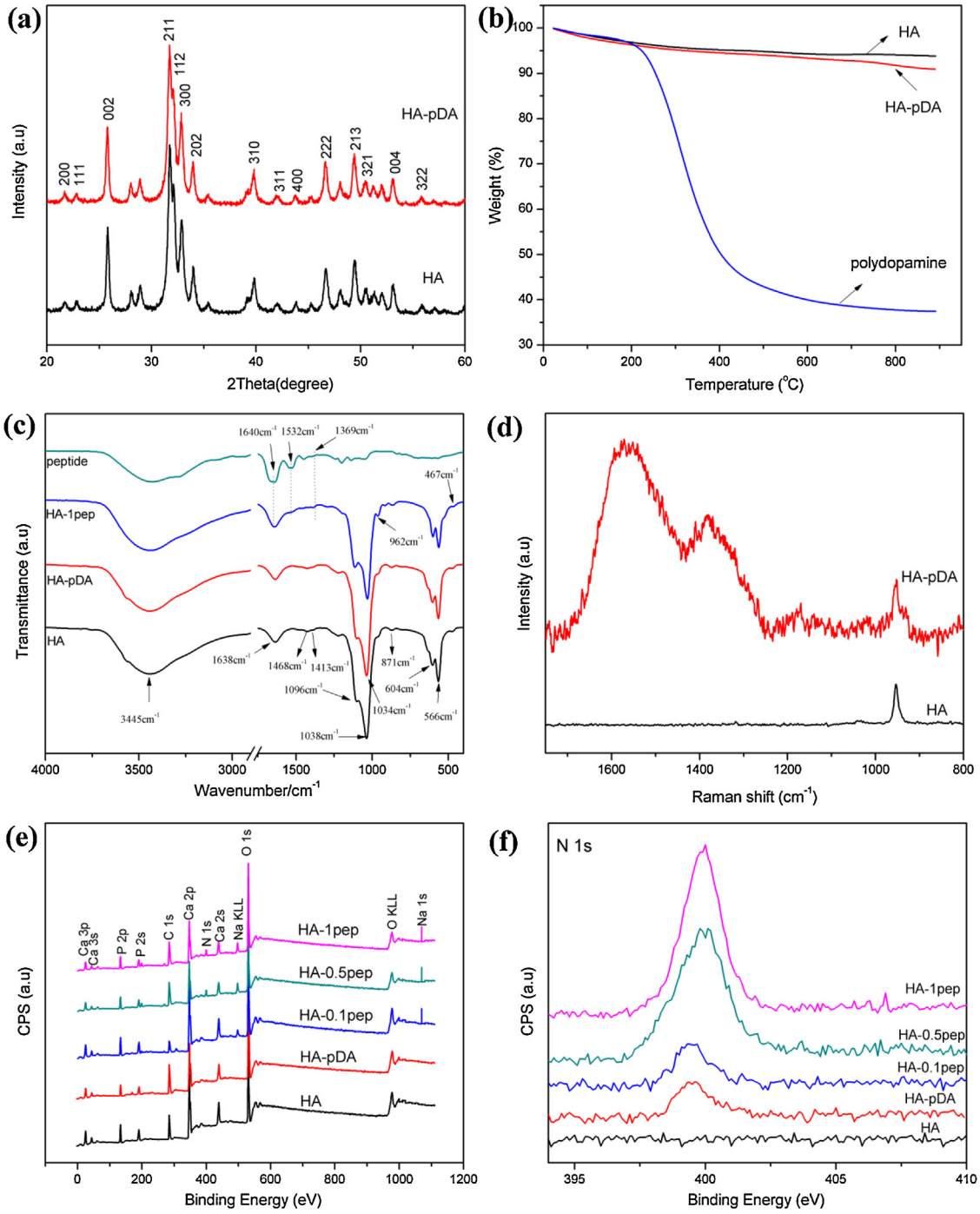

Fig. 2. XRD patterns (a), TG profiles (b) and Raman spectra (d) of the pristine HA and HA-pDA; FT-IR spectra (c) of the peptide, pristine nano-HA, HA-pDA and HA-1pep; XPS wide spectra (c) and high-resolution spectra of nitrogen peaks (N1s) (d) of all samples. (For interpretation of the references to spectra in figure legend, the reader is referred to the web version of the article.)

by hydrothermal treatment [31]. Then, the nano-HA was coated spontaneously by the formed pDA layer at pH 8.5 and 60 °C to obtain pDA coated HA (HA-pDA). The BMP-7 derived bone forming peptide was grafted onto the HA-pDA nanocrystals through the catechol chemistry, of which the thiols and amines of the biopolymers could react with the oxidized catechol groups *via* the Michael addition or Schiff base reactions.

3.1. Morphology analysis using TEM

The morphologies of the pristine nano-HA and the decorated HA nanocrystals were observed by TEM. Fig. 1a shows the typical rod-like particles, which is the characteristic structure of HA after hydrothermal treatment [32]. The lattice orientation of the HA nanoparticles in the HRTEM image is shown in Fig. S1a, with an interplanar distance of 0.281 nm, corresponding to the (2 1 1) planes of the HA hexagonal structure. To further verify the chemical composition of nano-HA, selected area electron diffraction (SAED) patterns and EDX analysis were carried out. The observed strong concentric ring patterns (the inset in Fig. 1a) could be assigned to the (0 0 2), (2 1 1) and (2 2 2) planes of HA, respectively. The Ca/P ratio of HA determined by EDX analysis (Fig. S1b), was about 1.65, slightly lower than the stoichiometric ratio of Ca/P in HA (≈1.67). The typical TEM micrograph of pDA is shown in Fig. 1b. Quantities

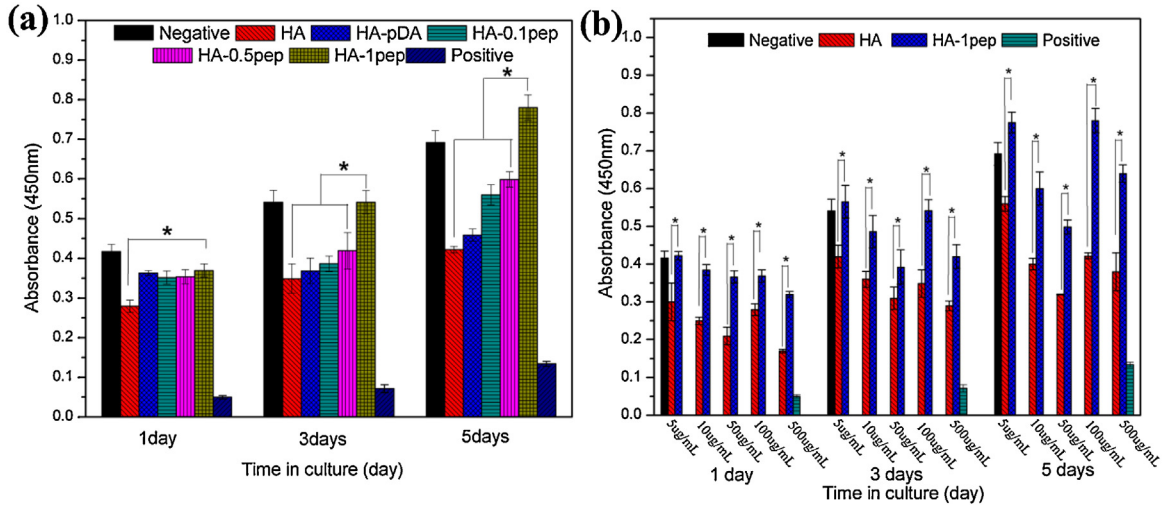

Fig. 3. The cell proliferation rates of MG-63 cells cultured for 1, 3, and 5 days, with the pristine nano-HA and different functionalized nano-HA (a), and with different concentrations of pristine nano-HA and HA-1pep (b). * represents $p < 0.05$.

of small spherical particles with the diameter of about 100–150 nm were seen. However, after coating pDA on HA surface, rod-like particles attached with distorted pDA spherical particle, and some clusters of HA particles appeared as displayed in Fig. 1c due to strong interfacial adhesion effect of pDA [27,28]. All samples were treated ultrasonically before TEM observation in our study. However, it was found that HA particles were less scattered out of the pDA layer, indicating a strong interaction between the HA particles and pDA. We could also observe that the images of the functionalized HA-1pep were clusters, similar to HA-pDA.

3.2. Chemical structure characterization

The phases of the as-prepared powders before and after pDA coating were investigated by XRD. The Bragg diffraction peaks of the pristine nano-HA, shown in Fig. 2a, matched quite well with those of the pure HA (PDF # 09-0432) at 2θ values of 25.8°, 31.7°, 32.9°, 46.7° and 49.5°, which were indexed to be (0 0 2), (2 1 1), (3 0 0), (2 2 2) and (2 1 3) planes, respectively [33,34]. Moreover, after pDA coating, the characteristic peak of HA did not change, indicating that pDA coating did not alter the crystallographic structure of nano-HA .

Thermal decomposition residue of pDA absorbed on the surface of HA can be identified by a weight loss. The TG profile in Fig. 2b indicated a dramatic 64.2% weight loss of the pDA from 150 °C to 500 °C, and pure nano-HA suffered a very slow weight loss process from room temperature to 900 °C. However, there was about 10% weight loss for the pDA coated HA powders with a lower thermal degradation rate compared with that of pure pDA, which was attributed to the decomposition of the grafted pDA. Due to the high thermal stability of HA [35], the incinerated residue of pDA-HA mainly consisted of HA. Therefore, after subtracting the water effect, the composition of HA-pDA sample was estimated to be about 6.6 wt% pDA and 93.4 wt% HA from the TG analysis.

The FT-IR spectra of the pristine HA and functionalized HA powders are shown in Fig. 2c. The typical broad peaks of OH^- were observed at 3445 cm^{-1}, and the peaks at 1638 cm^{-1} were also assigned to the absorbed H_2O. Existence of CO_3^{2-} originating from atmosphere observed at around 1468, 1413 cm^{-1} (ν_3) and 871 cm^{-1} (ν_2), clearly showed carbonate-substituted HA formation. The characteristic peak of PO_4^{3-} (ν_4) vibrations appeared at 566 cm^{-1} along with other ν_1, ν_2 and ν_3 phosphate peaks at 962, 467, 1096 and 1038 cm^{-1}, respectively. Moreover, the typical peak of pDA could not be detected in FT-IR spectra of HA-pDA, implying the extremely thin coating on the surface of nano-HA crystals. However, the stretching band of phosphate at 1038 cm^{-1} in the pristine HA shifted to 1034 cm^{-1} in HA-pDA sample, indicating the formation of strong interaction between the HA and the pDA molecule. Nevertheless, after the grafting of peptide, two new peaks at 1532 and 1369 cm^{-1} showed up, which should be assigned to the characteristic amide I ($\nu_{C=O}$) and the stretching vibration of carboxyl groups of peptide. In addition, the intensity of peaks was enhanced at about 1640 cm^{-1} which might result from the superimposed vibration of amide II (δ_{N-H}) and H_2O. These results indicated that the peptide was effectively covalently bonded on pDA-functionalized nano-HA. To further identify the existence of the pDA coating, Raman analysis was performed. For HA-pDA powders, the strong broad peaks at 1379 cm^{-1} (stretching of catechol) and 1565 cm^{-1} (deformation of catechol) appeared after pDA coating [36,37] in addition to intrinsic HA peaks at 958 cm^{-1} (Fig. 2d), suggesting that pDA was successfully coated on HA powders.

To verify the results obtained from the FT-IR and Raman analysis, XPS was applied to evaluate the detail chemical bonds formed on the surfaces of the functionalized HA. As shown in Fig. 2e, the pristine nano-HA exhibited carbon, oxygen, calcium, phosphorus peaks as the main atomic elements, whereas nitrogen and sodium peaks newly appeared in the XPS spectra for the peptide functionalized HA samples. The appearance of nitrogen signal (N1s) in the high-resolution narrow spectrum and their enhanced intensity with the increasing of the peptide concentration on the surface of nano-HA, indicated successful immobilization of the peptide. Furthermore, an evident change in carbon bond composition observed in the high-resolution narrow carbon spectra (C1s) clearly supported these conclusions (Fig. S2a–c). The high-resolution C1s spectrum of the pristine nano-HA was deconvoluted into three different curves. The binding energies centered at 284.8 eV, 286.4 eV and 289.0 eV were assigned to the carbon skeleton (—C—C—/—C—H—), hydroxyl group (—C—OH), carbonyl group (—C=O), respectively, whereas a broad peak —C—N— bond at about 285 eV was recorded on both HA-pDA and HA-1pep samples, indicating the presence of pDA and peptide. Additionally, after pDA coating, the intensity of the carbon skeleton (—C—C—/—C—H—) decreased dramatically, and the peaks of the hydroxyl, carbonyl group increased as shown in Fig. S2b. They should be attributed to the catechol group of HA-pDA. Compared with those of the HA-pDA, the peaks of the —C=O and —C—N— for the HA-1pep increased greatly in intensity due to abundant peptide bond (—NH—C=O) (Fig. S2c and d). The zeta potentials of the decorated HA were also measured. As shown in Table S1, the zeta

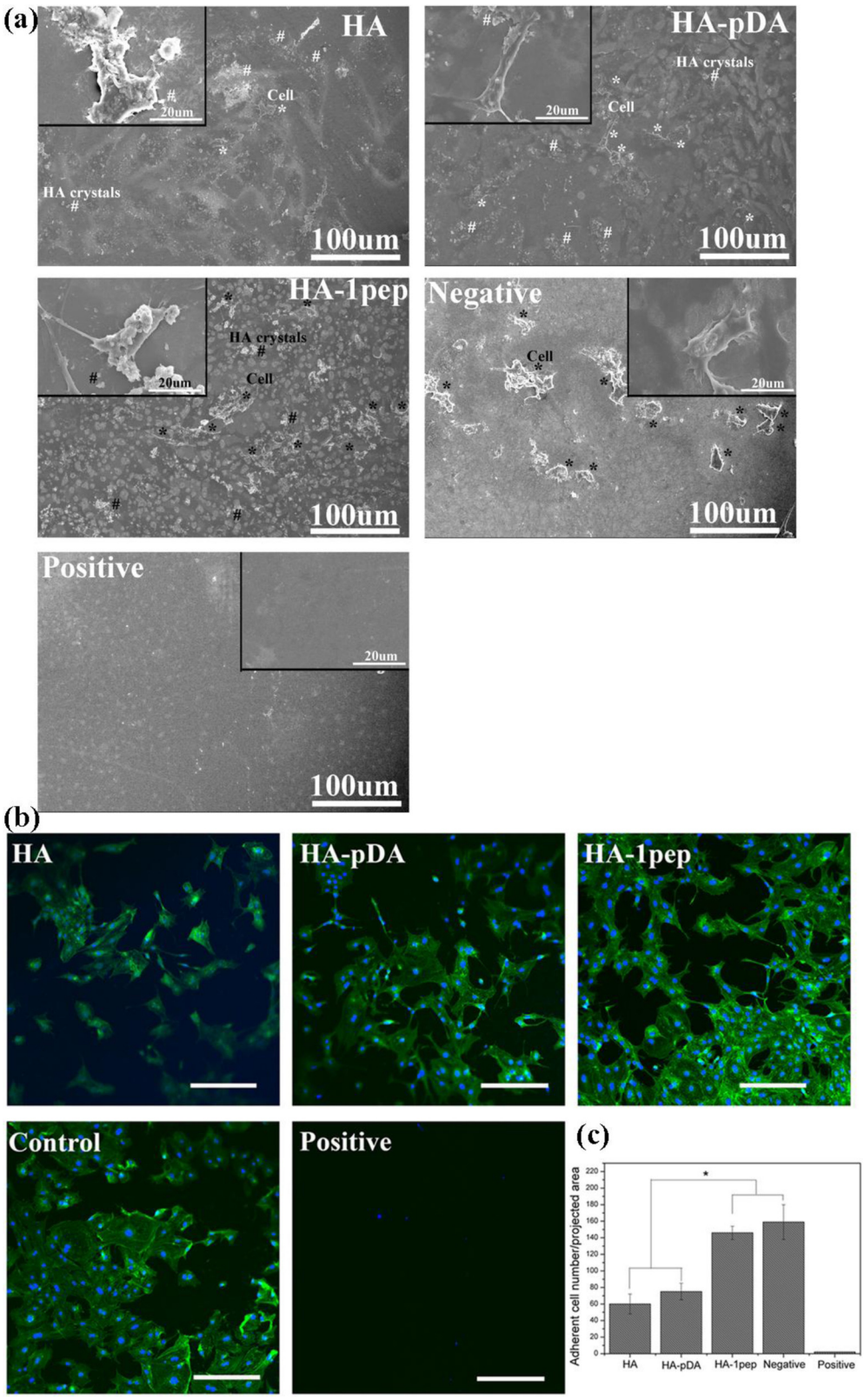

Fig. 4. SEM images of MG-63 (a); adhesion morphology and actin cytoskeletal organization (green, labeled with FITC-phalloidin, counterstained with DAPI for nuclei in blue) of MG-63 after incubation with pristine nano-HA and different nano-HA (b). Scale bar: 50 μm; (c) the number of adherent cells per projected area on the substrate. * represents $p < 0.05$. (For interpretation of the references to color in figure legend, the reader is referred to the web version of the article.)

potentials improved greatly after grafting peptide, which might be resulted from the successful decoration of the polar charged peptide.

3.3. Cell viability

In vitro biocompatibility of the peptide functionalized HA was investigated using CCK-8 assay on MG-63 cells. As shown in Fig. 3a, it was clear that the viability of cells co-cultured with the bone forming peptide functionalized HA displayed greatly statistical differences to the pristine HA group for 1 day, 3 days and 5 days, indicating that the peptide decorated HA could promote the cell proliferation. In addition, the osteoblasts viability increased with the increasing of the concentration of grafted peptide at 3 and 5 days, and the OD value of HA-1pep sample was about 1.9 times more than the pristine HA at 5 days. This suggested that HA-1pep strongly promoted the proliferation of MG-63 cells.

Moreover, the dose-dependent biocompatibility was tested with the pristine HA and HA-1pep for 1 day, 3 days, and 5 days. As shown in Fig. 3b, the pristine nano-HA presented an obvious dose-dependent cell proliferation, and the cell viability decreased with the increase of the nano-HA concentration in the range of 5–50 μg/mL, which were similar results to those reported by Xu et al. work [6]. The OD value of cell viability showed the lowest level under the concentration of 50 μg/mL. Nevertheless, at the concentration of 100 μg/mL, the cell viability improved again, and nano-HA was toxic at higher concentration of 500 μg/mL. It has been reported that nano-HA could inhibit the growth and promote the apoptosis of osteoblasts in a concentration-dependent manner [7,8]. The same phenomenon was observed in HA-1pep sample. However, when nano-HA was grafted with the peptide, the cell viability was much higher than pristine nano-HA in the whole ranges. Moreover, it was also noteworthy that HA-1pep at some concentration has higher cell viability than negative control at 5 days. These suggested that HA-1pep had clear advantages *in vitro* cell proliferation over the pristine nano-HA.

3.4. Cellular morphology and cytoskeletal observation

Previous reports demonstrated that pDA coating could enhance adhesion and survival of the cells [37,38] and promote the osteogenic differentiation [36]. To examine the function of the immobilized peptide on the pDA coated nano-HA, the next experiments were to measure adherent cell number and observe adherent morphology. Fig. 4a showed the numbers and morphologies of MG-63 growing with the pristine nano-HA and different functionalized nano-HA from SEM image. It could be seen that the cell numbers for HA-1pep groups were obviously enhanced compared to those of pristine nano-HA, which confirmed a good proliferation of HA-1pep, also shown from the optical microscope image (Fig. S3). Moreover, at the high magnification, the presence of abundant cellular filopodia demonstrated a better adhesion and spreading of osteoblast-like cells for HA-1pep group. The fluorescence images from Fig. 4b indicated that MG-63 showed limited spreading and displayed filamentous morphology on the pristine nano-HA powders, and F-actin was poorly developed. However, in HA-pDA group, MG-63 attached and spread more than the pristine nano-HA group, indicating that pDA coating could enhance cell adhesion, in accordance to previous reports. In comparison with the pristine nano-HA and HA-pDA samples, much more MG-63 cells adhered onto the bone forming peptide functionalized nano-HA group. Furthermore, as cell adhesion was enhanced, MG-63 cultured with HA-1pep group extended more adhered filopodia and spread more with visible presentation of more mature F-actin intracellular stress fibers (Fig. 4b). The number of adherent cells with HA-1pep group was significantly more than that of pristine nano-HA and HA-pDA groups,

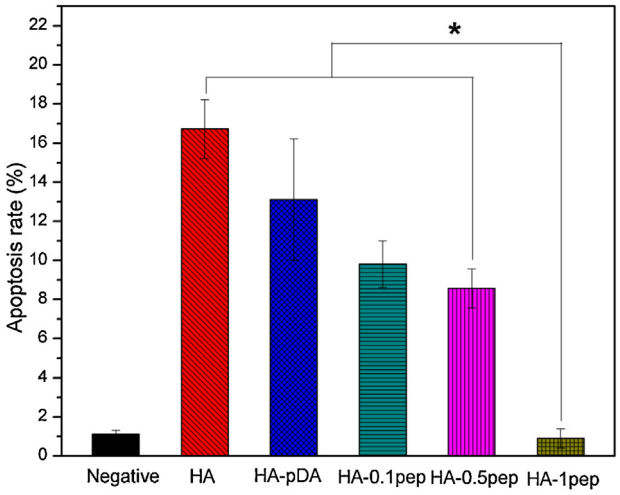

Fig. 5. Percentages of apoptotic cells determined from flow cytometric analyses. * represents $p < 0.05$.

indicating that HA-1pep exhibited excellent *in vitro* cytocompatibility.

3.5. Apoptosis analysis

Apoptosis and death of MG-63 cells were further detected using flow cytometry, with Annexin V-FITC/propidium iodide double-staining of cells. When MG-63 cells were treated with the pristine nano-HA and different functionalized nano-HA powders for 5 days, significant changes were found between the groups. Typical two-parameter figures for the flow cytometric analyses are shown in Fig. S3. From the images, we could see that more cells were located in B1 and B4 region for pristine nano-HA than other functionalized HA powders, implying a number of cells possessed the situation of early apoptosis and death. In addition, the extent of apoptosis was quantitatively analyzed by Summit 5.0 software. The apoptosis rate of nano-HA was measured to be 16.72% ± 1.5%, which was obviously higher than that of the functionalized nano-HA (Fig. 5). It was obvious that the apoptosis rate decreased as peptide concentration increased on the surface of pDA coated HA. Significant statistical differences between HA-1pep group and other groups, while little statistical differences between HA-1pep treated group and negative control group in apoptotic rates were noted in Fig. 5. These results suggested that the peptide functionalized nano-HA, especially at the peptide concentration of 1 mM, could prevent the apoptosis of MG-63 cells, which was in accord with the results from CCK-8 and cytoskeletal observation. There are several reports demonstrating peptide-modulated adhesion of bone cells by immobilized peptide. Chen et al. reported that a short peptide from BMP-7 enabled to increase osteoblast proliferation due to peptide–integrin interaction [39]. Balasundaram et al. has shown that anodised nanotubular titanium (TiO_2) bearing CKIPKASSVPTELSAISTLsYL peptides from BMP-2 enhanced the adhesion of human fetal osteoblasts [40]. Our results suggest that the combined effects of pDA and bone forming peptide might greatly promote the biological activity of the decorated nano-HA.

3.6. Alkaline phosphatase activity

In this paper, another goal is to present a general approach to endow the prepared nano-HA with high osteogenic differentiation activity to satisfy bone graft substitutes applications. Therefore, it is essential to examine the osteoblastic phenotypic expressions of the bone forming peptide grafted nano-HA. Alkaline phosphate (ALP) is

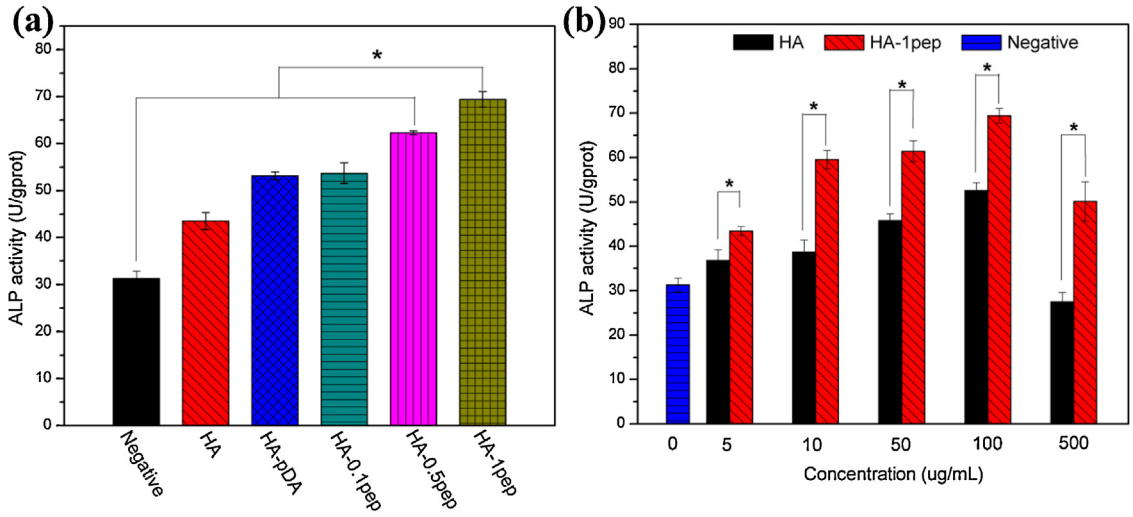

Fig. 6. ALP activity of MG-63 cells after cultivating for 7 days, with the pristine nano-HA and decorated nano-HA (a), and with different concentrations of pristine nano-HA and HA-1pep (b). *represents $p < 0.05$.

an important feature of osteoblast cells expressed in their differentiation phase and a significant quantitative marker of osteogenesis at 7–14 days [41]. *In vitro* ALP activities of MG-63 cells cultivating with the functionalized nano-HA were evaluated. As shown in Fig. 6, higher ALP activities have been obtained for MG-63 cells cultured with the pristine nano-HA and functionalized nano-HA than negative control. Additionally, the increased ALP expression was detected with the increasing of the peptide concentration, which indicated that the peptide functionalization of nano-HA with bone forming peptide could further enhance the mineralization and cell activation of the MG-63 cells. As mentioned above, the bone forming peptide from BMP-7 has been reported to greatly up-regulate biological markers during osteogenesis and enhance osteogenic differentiation of bone cells [24,42], therefore facilitating the formation of bone. The excellent osteogenic property of HA-1pep suggested that the grafted peptide remained its biological activity after immobilized onto the surface of HA-pDA.

The dose-dependent osteogenic activity was also tested by MG-63 cell cultured with different concentrations of the pristine nano-HA and HA-1pep groups for 7 days. Clearly, positive concentration-dependence properties could be observed. ALP activity was low at both low and high concentration of the pristine nano-HA and HA-1pep, because low concentration of powders could not stimulate the differentiation of MG-63 cells, and high concentration would inhibit the cell proliferation and cause the death of cell [7], as discussed in CCK-8 results. Nevertheless, higher ALP activities were seen for the MG-63 cells cultured with HA-1pep groups than the pristine nano-HA groups at each concentration. Inconsistent with CCK-8 assay results, the osteogenic activity of MG-63 increased from 0 to 50 μg/mL. However, the cell viability of MG-63 decreased with the increasing of the concentration of HA-1pep at the range of from 0 to 50 μg/mL. Combining these two factors, the 100 μg/mL of the peptide decorated HA was beneficial to both the viability and osteogenic differentiation of HA-1pep. As a consequence, our innovative peptide decoration using mussel-inspired pDA coating has endowed poorly bioactive nano-HA with both outstanding *in vitro* bone bioactivity and biocompatibility potential for bone repairing, bone regeneration, and bio-implant coating applications.

4. Conclusion

In summary, a novel peptide decorated nano-HA crystals with both enhanced bioactivity and osteogenic differentiation activity was prepared: immobilization of dopamine on the surface of nano-HA followed by one-step self-polymerization of dopamine, and the tethering of the bone forming peptide derived from BMP-7 *via* catechol chemistry. Fourier transform infrared spectrometry (FT-IR), X-ray photoelectron spectroscopy (XPS) and Zeta potential measurements confirmed that the peptide was successfully grafted onto the surface of nano-HA. After 3 days incubation, the peptide decorated nano-HA (HA-1pep) induced good *in vitro* cell proliferation toward MG-63 cells, especially at the concentration of 100 μg/mL. The immunofluorescence and apoptosis measurements revealed that the peptide functionalized HA-pDA exhibited excellent bioactivity. Moreover, biological activity of the grafted peptide could be maintained after immobilizing onto the surface of HA-pDA. Compared with the pristine nano-HA, the bone forming peptide decorated nano-HA improved both cell proliferation and cell differentiation in terms of the alkaline phosphatase activity. We believe that this facile biomimetic method offers a promising strategy for the fabrication of biopolymer modified nano-HA with immobilization of other osteogenetic or bioactive ligands, such as hyaluronic acid, enzyme, DNA, heparin and so on. Therefore, the biocompatible nano-HA with enhanced bioactivity and osteogenic differentiation activity is a promising candidate for bone graft substitutes and bio-implant coating applications.

Acknowledgments

This work was supported by Beijing Natural Science Foundation (7132124), State Key Development Program for Basic Research of China (Grant 2007CB936103), the Fundamental Research Funds for the Central Universities, and Peking University's 985 Grant.

Appendix A. Supplementary data

Supplementary data associated with this article can be found, in the online version, at http://dx.doi.org/10.1016/j.colsurfb.2013.05.037.

References

[1] R. Murugan, S. Ramakrishna, Compos. Sci. Technol. 65 (2005) 2385.
[2] J.R. Woodard, A.J. Hilldore, S.K. Lan, et al., Biomaterials 28 (2007) 45.
[3] D.Y. Lin, X.X. Wang, Colloids Surf. B: Biointerfaces 82 (2011) 637.
[4] A. Grandjean-Laquerriere, P. Laquerriere, D. Laurent-Maquin, et al., Biomaterials 25 (2004) 5921.
[5] P. Laquerriere, A. Grandjean-Laquerriere, E. Jallot, et al., Biomaterials 24 (2003) 2739.

[6] Z. Xu, J. Sun, C. Liu, J. Wei, Mater. Sci. Forum 610–613 (2009) 1364.
[7] M. Motskin, D.M. Wright, K. Muller, et al., Biomaterials 30 (2009) 3307.
[8] Q. Fu, N. Zhou, W. Huang, et al., J. Biomed. Mater. Res. A 74A (2005) 156.
[9] S. Ohba, W. Wang, S. Itoh, et al., Acta Biomater. 8 (2012) 2778.
[10] Y.J. Hong, J.S. Chun, W.K. Lee, Colloids Surf. B: Biointerfaces 83 (2011) 245.
[11] K. Balani, R. Anderson, T. Laha, et al., Biomaterials 28 (2007) 618.
[12] Y.-C. Kuo, C.-F. Yeh, Colloids Surf. B: Biointerfaces 82 (2011) 624.
[13] Y. Wu, S.R. Coyer, H. Ma, et al., Acta Biomater. 6 (2010) 2898.
[14] X. Chen, P. Sevilla, C. Aparicio, Colloids Surf. B: Biointerfaces 107 (2013) 189.
[15] S.M. Kang, B. Kong, E. Oh, et al., Colloids Surf. B: Biointerfaces 75 (2010) 385.
[16] Y. Ito, Soft Matter 4 (2008) 46.
[17] K. Yang, J.S. Lee, J. Kim, et al., Biomaterials 33 (2012) 6952.
[18] Z. Melkoumian, J.L. Weber, D.M. Weber, et al., Nat. Biotechnol. 28 (2010) 606.
[19] R. Luo, L. Tang, J. Wang, et al., Colloids Surf. B: Biointerfaces 106 (2013) 66.
[20] X. He, J. Ma, E. Jabbari, Langmuir 24 (2008) 12508.
[21] G. Bishop, T. Einhorn, Int. Orthop. 31 (2007) 721.
[22] S. Kann, R. Chiu, T. Ma, et al., J. Biomed. Mater. Res. A 94A (2010) 485.
[23] P. Yilgor, R. Sousa, R. Reis, et al., J. Mater. Sci. Mater. Med. 21 (2010) 2999.
[24] H.K. Kim, J.H. Kim, D.S. Park, et al., Biomaterials 33 (2012) 7057.
[25] H. Senta, E. Bergeron, O. Drevelle, et al., Can. J. Chem. Eng. 89 (2011) 227.
[26] J. Lock, H. Liu, Int. J. Nanomed. 6 (2011) 2769.
[27] H. Lee, S.M. Dellatore, W.M. Miller, et al., Science 318 (2007) 426.
[28] L.-P. Zhu, J.-H. Jiang, B.-K. Zhu, et al., Colloids Surf. B: Biointerfaces 86 (2011) 111.
[29] C.-Y. Chien, T.-Y. Liu, W.-H. Kuo, et al., J. Biomed. Mater. Res. A 101A (2013) 740.
[30] H.S. Yang, J. Park, W.G. La, et al., Tissue Eng. C 18 (2012) 245.
[31] X. Liu, M. Zhao, J. Lu, et al., Int. J. Nanomed. 7 (2012) 1239.
[32] Z. Xu, C. Liu, J. Wei, et al., J. Appl. Toxicol. 32 (2012) 429.
[33] Y. Deng, Y. Sun, X. Chen, et al., Mater. Sci. Eng. C 33 (2013) 2905.
[34] X. Li, J. Huang, M. Edirisinghe, et al., Colloids Surf. B: Biointerfaces 82 (2011) 562.
[35] T.I. Ivanova, O.V. Frank-Kamenetskaya, A.B. Kol'tsov, et al., J. Solid State Chem. 160 (2001) 340.
[36] N.G. Rim, S.J. Kim, Y.M. Shin, et al., Colloids Surf. B: Biointerfaces 91 (2012) 189.
[37] S.H. Ku, J. Ryu, S.K., et al., Biomaterials 31 (2010) 2535.
[38] Y.M. Shin, Y.B. Lee, H. Shin, Colloids Surf. B: Biointerfaces 87 (2011) 79.
[39] Y. Chen, T.J. Webster, J. Biomed. Mater. Res. A 91A (2009) 296.
[40] G. Balasundaram, C. Yao, T.J. Webster, J. Biomed. Mater. Res. A 84A (2008) 447.
[41] S. Hattar, A. Berdal, A. Asselin, et al., Eur. Cells Mater. 4 (2002) 61.
[42] J. Vlacic-Zischke, S.M. Hamlet, T. Friis, et al., Biomaterials 32 (2011) 665.